New Simplified Method for the Simulation of Conducted EMI Generated by Switched Power Converters

David González, *Member, IEEE*, Javier Gago, and Josep Balcells, *Member, IEEE*

***Abstract*—A new simplified simulation method for the calculation of conducted electromagnetic interference (EMI) caused by switched power converters (SPCs) is presented. EMI simulation in real SPCs presents particular problems due to complex geometry and the wide range of time constants involved. This makes the computation of EMI a complex matter. The method presented here is based on a "*source–propagation-path-derived disturbance*" simulation process and is specially designed to simplify the mentioned computation problems. In the design of the proposed method, quick and robust simulations were preferred rather than very accurate results. The resulting models allow quite accurate predictions and sensitivity analysis when certain changes in components or layout are introduced. The paper presents two validation cases, where simulation and experimental results of conducted EMI generated by a general-purpose VSI, with different switching patterns and different layout, are compared.**

***Index Terms*—Converters, electromagnetic interference (EMI), modeling, power conversion.**

I. Introduction

NOWADAYS, most electrical power used needs some kind of processing before being consumed. Almost all of this processing is done by switched power converters (SPCs), like rectifiers, inverters, dc/dc converters, etc., used in uninterruptible power systems (UPSs), variable-speed drives, active power filters, and many other applications. Such massive use of SPCs has some drawbacks, i.e., due to the inherent switching process, they have become one of the most important sources of electromagnetic interference (EMI) in the industrial environment. Several proposals have been made to reduce the problem, like the use of soft-switching techniques [1]–[3] or spread spectrum commutation patterns [4]. Nevertheless, hard switching is still playing a main role in electric power conversion [5].

The most relevant characteristics of SPC, from the EMI point of view, are the following.

1) *Many nonlinear components involved in a complex geometry*—Because of this, some common modeling techniques based on finite-difference time-domain (FDTD), method of moments (MoM), partial-element equivalent-circuit (PEEC), etc., used in the simulation of conducted and radiated EMI of printed circuit boards (PCBs) or even power systems [6]–[8], are not suitable for a commercial SPC with a complex geometrical structure [9], [10]. The main reasons are the complexity of the layout, the great number of different boundaries and the ignorance of many physical parameters related to propagation paths. Because of this, some recent works have searched for simplified methods for modeling EMI in SPCs [11]–[13].
2) *Wide range of time constants involved in SPC operation*—Three main groups of time constants can be distinguished. First, are those related to output fundamental frequency (approximate range $\tau > 1$ ms). A second group consists of time constants related to the switching frequency (approximate range $1\ \mu\text{s} < \tau < 1$ ss. The third group is related to rise and fall times and transients during switching (approximate range $10\text{ ns} < \tau < 1\ \mu$s). Because of this wide range of values, time domain simulations need very short calculation steps (long simulation periods) and wide tolerance margins, otherwise they have serious convergence problems.

Due to the above-mentioned problems, time domain does not seem to be a suitable approach for sensitivity analysis of certain components or layout parameters or for testing different modulation techniques. The use of frequency-domain techniques allows for overcoming the above-mentioned problems with significant advantages. According to Shannon's sampling theorem, to predict SPC EMI in the whole conducted band (10 kHz–30 MHz), all time constants greater than 15 ns should be considered. Instead, using frequency-domain techniques, the simulation complexity does not increase when the frequency range is extended. Accuracy of results depends only on the accuracy of *source* and *path* models. Moreover, in frequency-domain simulations, there is no need to cover the whole frequency range if desired. Simulations covering a restricted band, for example, 1 MHz, may be run by only considering time constants in the range of microseconds, with considerable savings in the *source* and *path* models complexity.

In order to illustrate the validity of the proposed methodology, we shall use it to analyze a very common problem in ac motor drives, i.e., the common-mode (CM) current circulation through the motor. Such current is the origin of many unwanted side effects, as described in [14] and [15]. Many different solutions can be found in the literature to fix this problem. Some of them propose a change of inverter structure [16], [17], while others are based on the use of special modulation techniques [18], [19]. Simulation tools presented here may help in the evaluation of effectiveness of such techniques.

Manuscript received August 27, 2002; revised June 21, 2003. Abstract published on the Internet September 17, 2003. This work was supported by the Comisión Interministerial de Ciencia y Tecnología under Project DPI 2001-2213.

The authors are with the Electronics Engineering Department, Universitat Politècnica de Catalunya, 08222 Terrassa, Spain (e-mail: dgonzalez@eel.upc.es; xgago@eel.upc.es; balcells@eel.upc.es).

Digital Object Identifier 10.1109/TIE.2003.819675

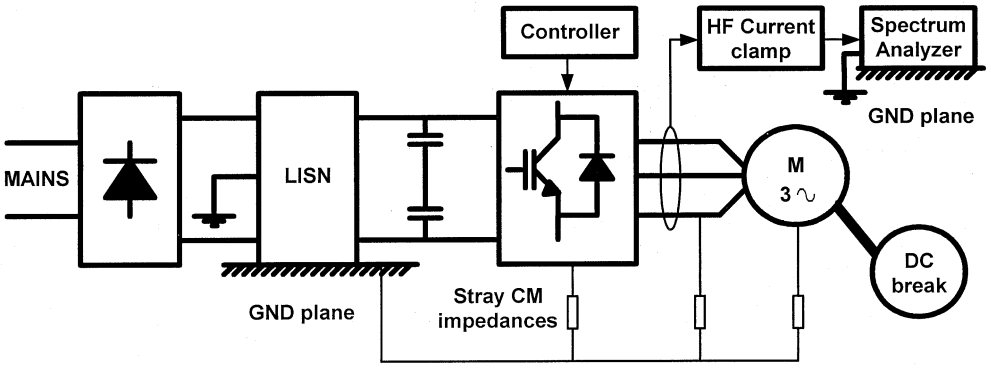

Fig. 1. Schematics of experimental plant.

II. Basics of Simplified Method

The proposed modeling method is based on the following basic assumptions.

1) *The model* is based on two equivalent circuits: one for differential mode (DM) and another for CM. No interaction is considered between DM and CM disturbances. This is approximately true if the power circuit has a good phase-to-phase and phase-to-ground symmetry, otherwise, the impedance unbalance in the CM circuit will cause DM disturbances. At a first stage we shall consider a good symmetry and, therefore, a perfect decoupling between DM and CM. In DM, stray couplings between live parts and ground are neglected, while in CM such couplings are considered the main propagation path.
2) *The sources*—DM disturbances are considered to be caused by sudden changes (di/dt) of load current flowing through inductive paths and will be modeled by current sources. CM disturbances are considered to be caused by sudden changes of voltage (di/dt) at certain points and will be modeled by voltage sources placed between such points and ground.
3) *Propagation paths* are described by a set of series and parallel impedances attributed to inductive paths and capacitive couplings, including ground. The first approach is based on lumped and time-invariant impedance models. The actual impedances to fill in the model may be measured as described in [19] and [20] or, in a first approach, estimated or evaluated by other methods like PEEC [6], [8]. Capacitive couplings are considered to be dominant, while inductive couplings may be neglected if reasonable care is taken to avoid current loops with a big surface area (twisted cables or multilayer buses). If not, mutual inductance couplings must be added to the equivalent circuit and complexity is increased.
4) *The switching pattern* is considered to be perfectly periodic. This is a pessimistic assumption, since the random changes in the period would decrease the EMI spectrum average [4].
5) *The resulting disturbance*—In the general case, the simulation process consists of the calculation of two current vectors, derived from the resolution of DM and CM equivalent circuits. Such current vectors allow the calculation of disturbance effects on a standard impedance network. We shall use a standard line-impedance stabilization network (LISN) for this purpose, which will additionally provide the means to isolate the SPC from other possible sources of disturbances.

Models obtained with the above-described method are very useful to the designer in assessment tasks in order to quickly answer questions like *"Which is the cause of noncompliance, DM or CM?"* or *"What to do to improve EMI behavior in the converter?"* or *"How effective a certain filter. . .or decoupling capacitor will be?"* The model is intended to provide quick and robust simulations, which at this point of the design are preferred rather than very accurate results [20]. A similar approach, using state variable techniques, has been proposed recently in [13]. However, in the state variable approach, all energy storage components, L and C, even the stray ones, must be considered in the model and each generates at least one state variable. Because of that, the model complexity is relatively high, even for very simple circuits (state vectors with many components). To have a rough idea, the model of a simplified single-switch converter used in [13] needs 12 significant state variables. Some of the considered state variables cannot be assigned to any component or layout parameter, and therefore they do not provide information on *"What to improve."* For sensitivity studies, the simplified method presented here allows the simulation of even more complex systems with a smaller number of equations.

III. Experimental Plant Description

In order to show the features of the proposed simulation method, it has been used to evaluate conducted EMI in a commercial variable-frequency drive for speed control of ac motors. A simplified schematic of the experimental plant is shown in Fig. 1. Fig. 2 shows a more detailed schematic of the inverter, showing the main elements and some relevant stray propagation paths. Since we wanted to evaluate EMI produced by the inverter alone (not the rectifier), a standard LISN was placed at the dc bus. This allows repeatable measurements and also the comparison of the proposed method with other standard test methods. In fact, if commutation effects of the rectifier can be neglected, EMI at the ac mains side is the same as at the dc bus, but modulated by the six-pulse commutation of the rectifier [20]. Since the modulation is at low frequency (300 Hz in a 50-Hz mains), side bands of modulation cannot be distinguished with the standard resolution

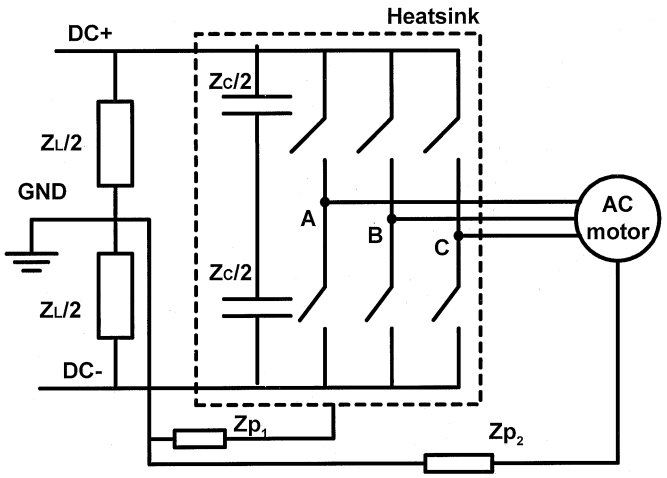

Fig. 2. Diagram of the experimental plant.

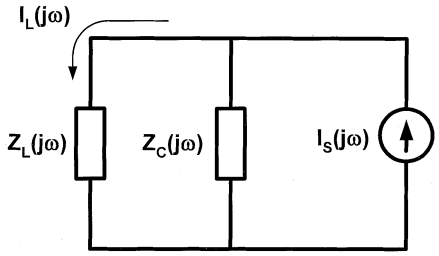

Fig. 3. DM equivalent circuit.

bandwidth for EMI measuring (9 kHz in the A band, or 120 kHz in the B band). Therefore, we can measure with the LISN at the dc side and still have the same results produced by the inverter at the mains side.

Notice as well that the layout of the converter was not simplified at all, in order to have a simpler geometry. Simplifications in the proposed model consist only of considering or neglecting certain sources of disturbance or making certain propagation path approximations.

IV. Application of the Proposed Method

As stated in Section II, the method is based on two equivalent circuits, for DM and for CM, respectively.

A. DM Model

According to simplifications explained in Section II, the DM equivalent circuit can neglect all the stray couplings between live parts and ground. The source of disturbances is considered to be the load current. The resulting DM simplified equivalent circuit is shown in Fig. 3, where Z_L is the impedance of the LISN, Z_C is the impedance of the dc bus (including stray components), I_S is the load current (EMI source), and I_L is the current through the LISN (simulation result).

The source of disturbance I_S can be calculated from the output voltage V_0 divided by the load impedance Z_L as stated in (1). V_0 is derived from the pulsewidth-modulation (PWM) pattern, which has been represented in Fig. 4. For a first approach, infinite slope pulses may be considered, but this allows only rough predictions in the A band (10–150 kHz). If

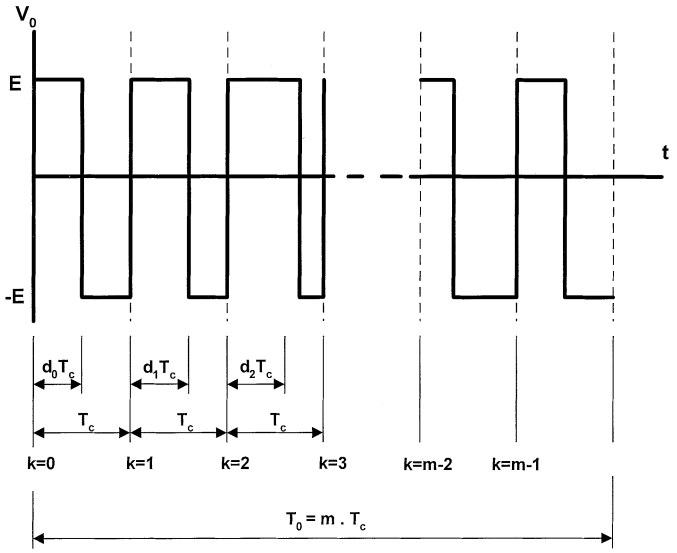

Fig. 4. Inverter output voltage V_0.

V_0 is defined as a sequence of finite slope pulses, where rise and fall times, t_r and t_f, are evaluated from real behavior or from a short time-domain simulation, good predictions can be done up to a few megahertz. Time- and frequency-domain expressions of V_0, considering the latter case, are given in (2) and (3), respectively. Later experimental results reveal that if good predictions in the whole B band (150 kHz–30 MHz) are desired, a more precise function of $V_0(t)$ during commutation has to be obtained and included in the model by a convolution process as in [21]

$$I_S(j\omega) = \frac{V_0(j\omega)}{Z_0(j\omega)} \tag{1}$$

$$\begin{aligned} V_0(t) = 2E \cdot \sum_{k=0}^{k=m-1} \Bigg[& \frac{1}{t_r}(u(t-kT_c)(t-kT_c) \\ & + u(t-kT_c-t_r)(kT_c+t_r-t)) \\ & + \frac{1}{t_f}(u(t-(k+d_k)T_c) \\ & \cdot ((k+d_k)T_c - t) \\ & + u(t-(k+d_k)T_c-t_f) \\ & \cdot (t-(k+d_k)T_c-t_f) \Bigg] \end{aligned} \tag{2}$$

$$\begin{aligned} V_0(n\omega_0) = \frac{2E}{jn\omega_0} \sum_{k=0}^{k=m-1} \Bigg(& e^{-jkT_cn\omega_0} \Bigg(\frac{1}{jn\omega_0 t_r}(1-e^{-jt_rn\omega_0}) \\ & + \frac{e^{-jd_kT_cn\omega_0}}{jn\omega_0 t_f}(e^{-jt_fn\omega_0}-1) \\ & + e^{-jt_rn\omega_0}\left(1+\frac{kT_c}{t_r}\right) \\ & - \frac{kT_c}{t_r} + e^{-jd_kT_cn\omega_0} \\ & \times \left(\frac{(k+d_k)T_c}{t_f} - e^{-jt_fn\omega_0} \right. \\ & \left. \times \left(1+\frac{(k+d_k)T_c}{t_f}\right)\right)\Bigg). \end{aligned} \tag{3}$$

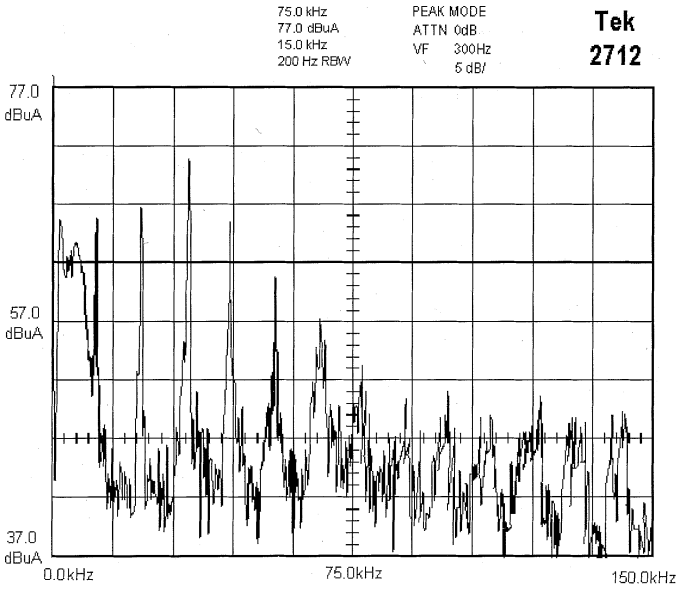

Fig. 5. Experimental DM current spectrum.

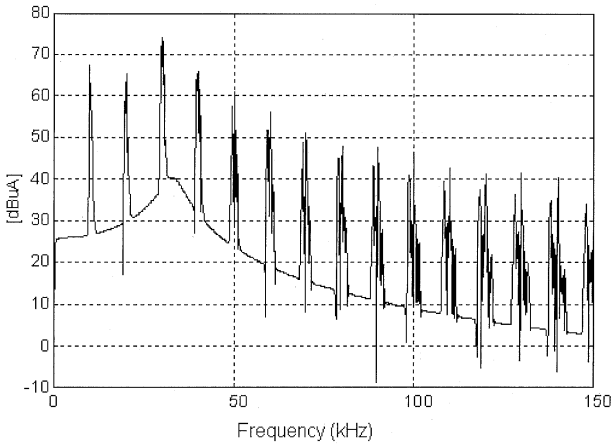

Fig. 6. Simulated DM current spectrum.

The comparison between DM simulated and experimental was established by comparing the current I_L sensed by an HF current clamp at the LISN and I_L given by (4), derived from the equivalent circuit in Fig. 4. Notice that measurement by means of an HF current clamp allows DM and CM signals to be separated

$$I_L(j\omega) = I_S(j\omega)\frac{Z_C(j\omega)}{Z_C(j\omega) + Z_L(j\omega)}. \tag{4}$$

Fig. 5 shows the EMI spectrum measured in the A band by an HF current clamp with 1 μA/1 μV ratio. This experimental spectrum should be compared with the simulation results shown in Fig. 6. In order to make the comparison easier, Table I shows the simulated and experimental values of the first ten harmonics of switching frequency. The last row shows the difference between simulated and experimental results.

It may be seen that comparison in band A shows a good concordance of results, with a maximum deviation of about 6 dB, which is close to the uncertainty of the test site. Concordance is maintained in band B up to 5 MHz approximately with acceptable deviations. New investigations revealed that the discordance is mainly due to simplifications in impedance modeling

TABLE I
SIMULATED AND EXPERIMENTAL DM CURRENT COMPARISON

Harmonics Order	1st	2nd	3rd	4th	5th	6th	7th	8th	9th	10th
SIM.[dB]	67	65	72	65	58	56	50	48	47	43
EXP.[dB]	66	67	76	66	61	57	53	51	51	49
$\lvert\Delta\rvert$ [dB]	1	2	4	1	3	1	3	3	4	6

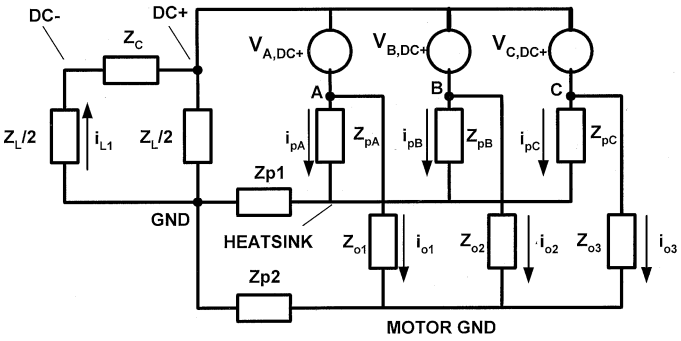

Fig. 7. CM equivalent circuit.

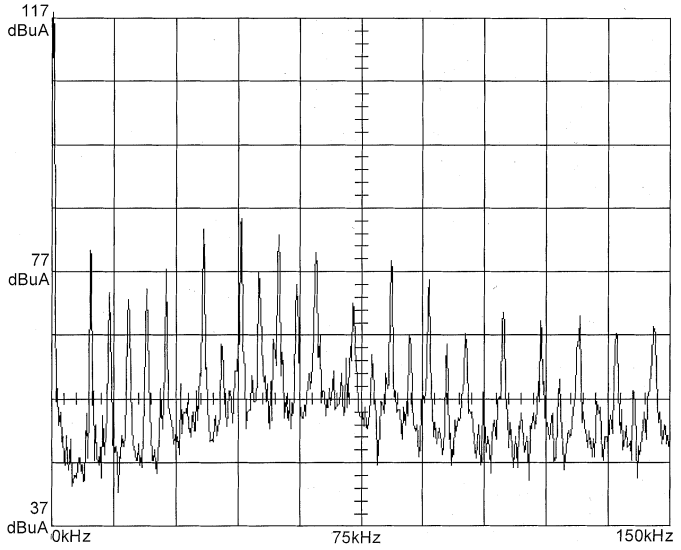

Fig. 8. CM current for CSVM (experimental).

the propagation path and in the source model considered in the example [20].

B. CM Model

The CM equivalent circuit is given in Fig. 7. As stated above, sources of EMI are considered to be the voltages at the midpoints of phase legs, i.e., points A, B, and C, where high dv/dt are found. Such points are connected to DC+ and DC− according to the switching pattern. Impedances to be considered include all the impedances (real and stray capacitive couplings) connecting live parts to ground. The detail of impedances in Fig. 8 is as follows. Sources are considered to be connected to DC+. Z_{pA}, Z_{pB}, and Z_{pC} are stray impedances between leg midpoints A, B, and C and the heat sink; Z_{o1}, Z_{o2}, and Z_{o3} are the CM impedances of load (motor in the present example); Z_{p1} is the impedance between heat sink and midpoint of the LISN;

Z_{p2} is the impedance between motor case and midpoint of the LISN; Z_L is the impedance of the LISN (theoretically 50 Ω in the band of interest) and $Z_{\rm DC}$ is the dc-bus impedance. Solving the net of Fig. 6 results in the equation system (5) and (6). The disturbing currents can then be derived from (7). See (5)–(7), shown at the bottom of the page. Notice that the *source–propagation path–disturbance* approach is clearly reflected in the above equations. The source is represented by vector $[V]$, the propagation path by the impedance matrix $[P]$, and the disturbance by current vector $[I]$. By using this approach, it is very easy to predict the influence of different switching patterns or the consequences of certain layout changes. This can be done by simply changing the source vector $[V]$ or the components of impedance matrix $[P]$, respectively. Section V presents an application example.

V. Model Validation: CM Current Simulation

The proposed method is used to show the influence of two factors on CM EMI generated by the above analyzed frequency converter. The evaluated factors are the following.

1) *PWM switching pattern*—This represents a change on vector $[V]$. Two different modulation techniques are compared: the Classical Space-Vector Modulation (CSVM) and the Common-Mode Reduction SVM (CMRSVM). The CMRSVM has been specially designed to cancel the CM voltage source between motor case and dc midpoint (LISN midpoint) in a three-phase inverter. These modulation techniques are thoroughly explained and compared in [18] and [22].
2) *The effect of a change in system layout*: connection/disconnection of a direct link conductor between the motor case and ground, which means a change on the impedance *Z_{p2}* of matrix $[P]$.

A. Modulation Techniques Comparison

CM current at the protective conductor in identical conditions ($f_o = 25$ Hz, $f_{\rm switching} = 9$ kHz) has been measured with an HF current clamp for both modulation techniques, CSVM and CMRSVM. Measured spectrums are shown in Figs. 8 and 9, and should be compared with simulation results, shown in Figs. 10 and 11. The comparison shows a good agreement, especially above 50 kHz. In this range of frequencies the error is less than 5 dB (close to the uncertainty of the site). In the CMRSVM case and for frequencies above 50 kHz, the simulation provides values that are smaller than the background noise, therefore, harmonics of switching frequency do not appear in the experimental measurement.

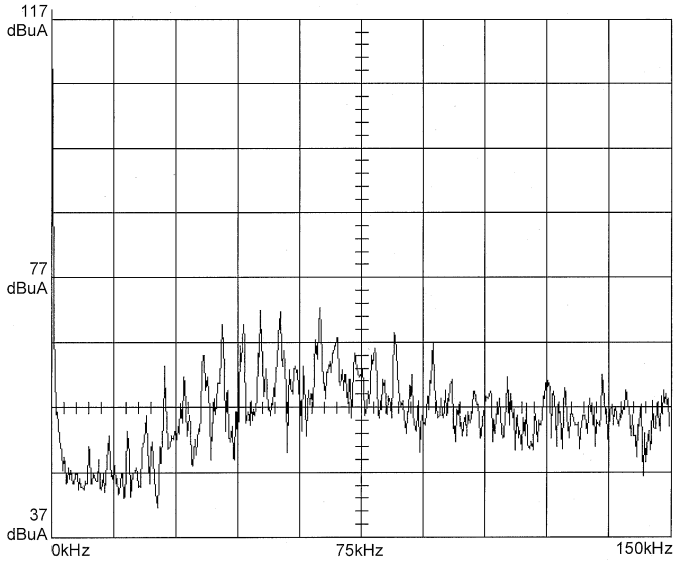

Fig. 9. CM current for CMRSVM (experimental).

B. Layout Case Comparison

Fig. 12 shows the CM current difference between two cases: with and without a direct link conductor connected between the motor case and system ground (GND) and Fig. 13 shows simulated results under the same conditions. In order to make the comparison easier, Table II shows simulated and experimental

$$\begin{pmatrix} V_{A,\rm DC+} \\ V_{B,\rm DC+} \\ V_{A,\rm DC+} - V_{B,\rm DC+} \\ 0 \\ 0 \\ 0 \\ V_{C,\rm DC+} - V_{B,\rm DC+} \end{pmatrix} = [P] \cdot \begin{pmatrix} i_{pA} \\ i_{pB} \\ i_{pC} \\ i_{o1} \\ i_{o2} \\ i_{o3} \\ i_{L1} \end{pmatrix} \tag{5}$$

$$[p] = \begin{pmatrix} Z_{p1}+Z_{pA} & Z_{p1} & Z_{p1} & 0 & 0 & 0 & \frac{Z_L}{2}+Z_{\rm DC} \\ Z_{p1}+\frac{Z_L}{2} & Z_{p1}+\frac{Z_L}{2}+Z_{pB} & Z_{p1}+\frac{Z_L}{2} & \frac{Z_L}{2} & \frac{Z_L}{2} & \frac{Z_L}{2} & -\frac{Z_L}{2} \\ 0 & 0 & 0 & -Z_{o1} & Z_{o2} & 0 & 0 \\ -Z_{p1} & -Z_{p1} & -(Z_{p1}+Z_{pC}) & Z_{p2} & Z_{p2} & Z_{p2}+Z_{o3} & 0 \\ Z_{pA} & -Z_{pB} & 0 & -Z_{o1} & Z_{o2} & 0 & 0 \\ -\frac{Z_L}{2} & -\frac{Z_L}{2} & -\frac{Z_L}{2} & -\frac{Z_L}{2} & -\frac{Z_L}{2} & Z_{\rm DC}+Z_L & 0 \\ -Z_{p1} & -(Z_{p1}+Z_{pB}) & -Z_{p1} & Z_{p2} & Z_{p2} & Z_{p2}+Z_{o3} & 0 \end{pmatrix} \tag{6}$$

$$[I] = [P]^{-1} \cdot [V] \tag{7}$$

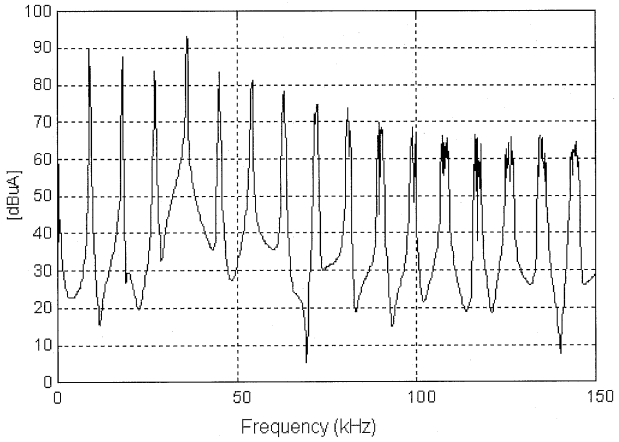

Fig. 10. CM current for CSVM (simulation).

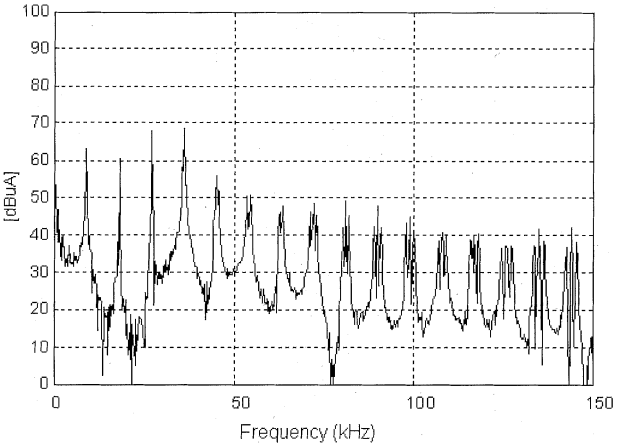

Fig. 11. CM current for CMRSVM (simulation).

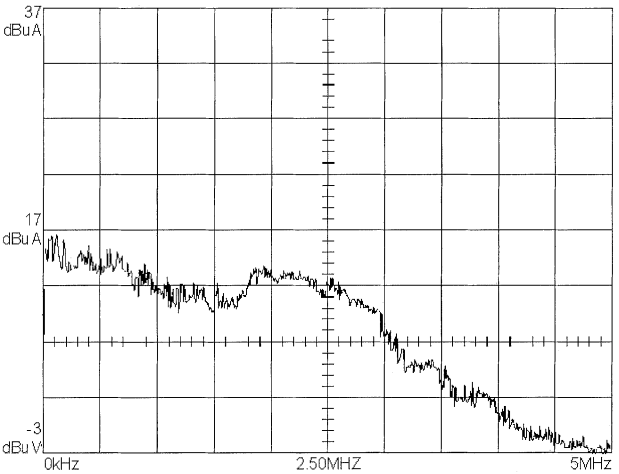

Fig. 12. CM current difference with the link connected/disconnected (experimental).

results and the last row shows the difference between both. Notice that there is a good concordance, well within the uncertainty limits of the site and measuring equipment.

At low frequencies the link disconnection causes an important reduction of CM current as could be intuitively expected, but at high frequencies the stray capacitance coupling makes the difference insignificant. Nevertheless, due to a resonance, an unexpected increase of EMI appeared at frequencies between 3.5–4.5 MHz. This effect was clearly predicted by the model.

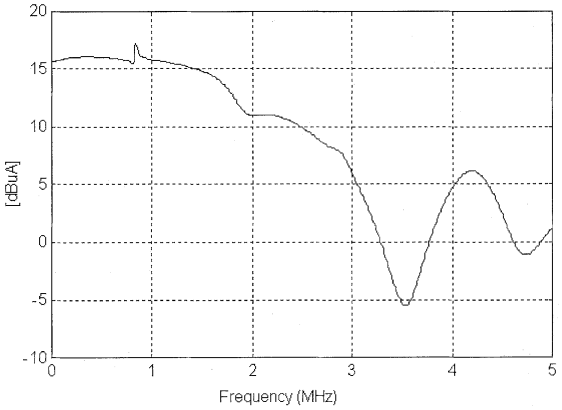

Fig. 13. CM current difference with the link connected/disconnected (simulated).

TABLE II
SIMULATED AND EXPERIMENTAL DIFFERENCES WITH/WITHOUT PROTECTIVE CONDUCTOR

f(MHz)	**0.5**	**1**	**1.5**	**2**	**2.5**	**3**	**3.5**	**4**	**4.5**	**5**
SIM [dB]	*+16*	*+16*	*+15*	*+11*	*+10*	*+6*	*-5*	*+5*	*+2,5*	*+1*
EXP [dB]	*+13*	*+12*	*+11*	*+13*	*+12*	*+8*	*+3*	*+2*	*0*	*-1*
$\lvert\Delta\rvert$ [dB]	*3*	*4*	*4*	*2*	*2*	*2*	*8*	*3*	*2.5*	*2*

VI. CONCLUSION

A new method for conducted EMI prediction in an SPC, using frequency-domain techniques applied to simplified equivalent circuits has been proposed and tested. The frequency-domain approach provides quick and robust simulations and avoids problems of convergence, which are typical in time-domain simulations. The agreement between simulated and experimental results is well within the uncertainty limits of the site and the measuring equipment up to 5 MHz. That means a good tradeoff between simplicity and accuracy of the model. The model uses a *source–propagation path–disturbance* calculation structure which facilitates the prediction of influence on emitted EMI of different modulation techniques or converter layout changes and allows sensitivity calculations, which may be very useful to achieve new improvements on already built equipment.

REFERENCES

[1] G. Hua and F. C. Lee, "An overall view of soft-switching techniques for power converters," *EPE Electron. J.*, vol. 3, no. 1, pp. 43–51, 1993.
[2] H. Chung, S. Y. R. Hui, and K. K. Tse, "Reduction of power converter EMI emission using soft-switching techniques," *IEEE Trans. Electromagn. Compat.*, vol. 40, pp. 282–287, Aug. 1998.
[3] G. Hua and F. C. Lee, "Soft-switching techniques in PWM converters," *IEEE Trans. Ind. Electron.*, vol. 42, pp. 595–603, Dec. 1995.
[4] "Implementing random space vector modulation with the ADMCF32X," Analog Devices, Norwood, MA, Applicat. Note ANF32X-54, 2000.
[5] D. Zhang, D. Y. Chen, and F. C. Lee, "An experimental comparison of conducted EMI emissions between zero-voltage transition circuit and a hard switching circuit," in *Proc. IEEE PESC'96*, 1996, pp. 1992–1996.

[6] M. Youssef, G. Antonini, E. Clavel, J. Roudet, S. Cristina, and A. Orlandi, "Conducted and radiated EMI characterization of power electronics converter," in *Proc. IEEE ISIE'97*, 1997, pp. SS207–SS211.
[7] G. Antonini, S. Cristina, and A. Orlandi, "EMC characterization of SMPS devices: Circuit and radiated emissions model," *IEEE Trans. Electromagn. Compat.*, vol. 38, pp. 300–309, Aug. 1996.
[8] G. Antonini, A. Orlandi, and A. E. Ruehli, "Harten's scheme for PEEC method," in *Proc. IEEE EMC Symp.*, 2001, pp. 340–344.
[9] J. Fan, J. L. Drewniak, H. Shi, and J. L. Knighten, "DC power bus modeling and design with a mixed potential integral equation formulation and circuit extraction," *IEEE Trans. Electromagn. Compat.*, vol. 43, pp. 426–436, Nov. 2001.
[10] B. Archambeault, S. Pratapneni, D. C. Wittwer, L. Zhang, and J. Chen. A Proposed Set of Specific Standard EMC Problems to Help Engineers Evaluate EMC Modeling Tools. IBM, Dell Computer Corp., Intel Corp.; IEEE EMC Society TC9. [Online]. Available: http://www.ewh.ieee.org/cmte/tc9/summary/summary.html
[11] F. Costa, E. Labouré, and V. Lavabre, "Validation of numerical calculations of the conducted and radiated emissions: Application to a variable speed drive," in *Proc. IEEE PESC'00*, 2000, pp. 934–939.
[12] C. Seporta, G. Tine, G. Vitale, and M. C. Di Piazza, "Conducted EMI in power converters feeding ac motors: Experimental investigation and modeling," in *Proc. IEEE ISIE'00*, 2000, pp. 359–364.
[13] P. R. Mugur, J. Roudet, and J. C. Crebier, "Power electronic converter EMC analysis through state variable approach techniques," *IEEE Trans. Electromagn. Compat.*, vol. 43, pp. 229–238, May 2001.
[14] D. Busse *et al.*, "The effects of PWM voltage source inverters on the mechanical performance of rolling bearings," in *Proc. IEEE APEC'96*, 1996, pp. 561–569.
[15] E. Zhong and T. A. Lipo, "Improvements in EMC performance of inverter-fed motor drives," *IEEE Trans. Ind. Applicat.*, vol. 31, pp. 1247–1256, Nov./Dec. 1995.
[16] T. Shimizu and G. Kimura, "High frequency leakage current reduction based on a common-mode voltage compensation circuit," in *Proc. IEEE PESC'96*, 1996, pp. 1961–1967.
[17] A. L. Julian, T. A. Lipo, and G. Oriti, "Elimination of common mode voltage in three phase simunoidal power converters," in *Proc. IEEE PESC'96*, 1996, pp. 1968–1972.
[18] M. Cacciato, A. Consoli, G. Scarcella, and A. Testa, "Reduction of common mode currents in PWM inverter motor drives," *IEEE Trans. Ind. Applicat.*, vol. 35, pp. 469–476, Mar./Apr. 1999.
[19] D. González, J. Gago, and J. Balcells, "Common mode EMI prediction for three-phase inverter," in *Proc. 9th European Conf. Power Electronics and Applications, EPE'01*, 2001, CD-ROM.
[20] D. González, "Caracterización de las estructuras, control y lay-out de convertidores conmutados para la reducción de perturbaciones," Ph.D. dissertation, Electron. Eng. Dept., Univ. Politècnica Catalunya, Terrassa, Spain, 2001.
[21] J. Balcells, D. González, M. Lamich, and D. Bedford, "EMI generation models for switched mode power supplies," in *Proc. European Space Power Conf.*, Sept. 1998, pp. 421–426.
[22] D. Gonzalez, J. Llaquet, A. Arias, D. Bedford, J. L. Romeral, and J. Balcells, "Improvement possibilities of PWM voltage inverter EMI effects using different modulation methods," in *Proc. 8th European Conf. Power Electronics and Applications, EPE'99*, 1999, CD-ROM.

David González (M'96) was born in Cerdanyola del Vallès, Spain, in 1968. He received the Master of Engineering and Doctoral degrees fron the Universitat Politècnica de Catalunya, Terrassa, Spain, in 1993 and 2001, respectively.

Since 1995, he has been an Assistant Professor in the Electronics Engineering Department, Universitat Politècnica de Catalunya. His topics of interest are electromagnetic compatibility in industrial electronics, HF modeling of switched converters, and power conversion and power quality.

Javier Gago was born in Barcelona, Spain, in 1965. He received the Master of Engineering and Doctoral degrees fron the Universitat Politècnica de Catalunya, Terrassa, Spain, in 1991 and 2003, respectively.

Since 1993 he has been an Assistant Professor in the Electronics Engineering Department, Universitat Politècnica de Catalunya. His topics of interest are electromagnetic compatibility, HF modeling of analog and digital ICs, PCB modeling, and instrumentation.

Josep Balcells (M'95) was born in Vila-Rodona, Spain, in 1949. He received the Master of Engineering and Doctoral degrees from the Universitat Politècnica de Catalunya, Terrassa, Spain, in 1975 and 1983, respectively.

From 1975 to 1986, he was an Associate Professor in the Electronics Engineering Department, Universitat Politècnica de Catalunya, where, since 1986, he has been a Ptofessor. From 1978 to 1986, he was the head of R&D in Power Elecronics with Agut (now a GE group company). He has led several research projects funded by the Comisión Interministerial de Ciencia y Tecnología and also by the European Union in the V Frame Program. His topics of interest are EMC in power systems, measurement and filtering of disturbances produced by power converters, and design of EMC-compliant power converters.